

# Ground-Motion Attenuation Relationships for Cascadia Subduction Zone Megathrust Earthquakes Based on a Stochastic Finite-Fault Model

by Nicholas J. Gregor, Walter J. Silva, Ivan G. Wong, and Robert R. Youngs

**Abstract** The number of strong ground motion recordings available for regression analysis in developing empirical attenuation relationships has rapidly grown in the last 10 years. However, the dearth of strong-motion data from the Cascadia subduction zone has limited this development of relationships for the Cascadia subduction zone megathrust, which can be used in the calculation of design spectra for engineered structures. A stochastic finite-fault ground-motion model has been used to simulate ground motions for moment magnitude ( $M$ ) 8.0, 8.5, and 9.0 megathrust earthquakes along the Cascadia subduction zone for both rock- and soil-site conditions. The stochastic finite-fault model was validated against the 1985  $M$  8.0 Michoacan, Mexico, and the 1985  $M$  8.0 Valpariso, Chile, earthquakes. These two subduction zone megathrust earthquakes were recorded at several rock sites located near the fault rupture. For the Cascadia megathrust earthquakes, three different rupture geometries were used to model the  $M$  8.0, 8.5, and 9.0 events. The geometries only differ in their respective fault lengths. A fault dip of  $9^\circ$  to the east with a rupture width of 90 km was selected to represent average properties of the Cascadia subduction zone geometry. A regional crustal damping and velocity model was used with the stochastic finite-fault model simulations. Ground motions were computed for 16 site locations. The parametric uncertainties associated with the variation in source, path, and site effects were included in the development of the ground motions. A functional form was fit to the ground-motion model simulations to develop region-specific attenuation relationships for the Cascadia megathrust rupture zone for both rock and soil site conditions. The total uncertainty was based on a combination of the modeling and parametric uncertainties (sigmas). These newly developed attenuation relationships for Cascadia subduction zone megathrust earthquakes can be used in both the probabilistic and deterministic seismic-hazard studies for engineering design for the Pacific Northwest.

## Introduction

The prediction of strong ground shaking in the Pacific Northwest from a great megathrust (interface) earthquake rupturing the Cascadia subduction zone is hampered by the absence of empirical data. Until recently, the only significant strong-motion data for the region were the recordings of the 1949 surface magnitude ( $M_s$ ) 7.1 Olympia and the 1965 body-wave magnitude ( $m_b$ ) 6.5 Seattle–Tacoma intraplate earthquakes and the 1992 moment magnitude ( $M$ ) 7.2 Cape Mendocino, California, earthquake at the south end of the Cascadia subduction zone. The recent 28 February 2001  $M$  6.8 Nisqually intraplate earthquake has increased the total number of strong ground motion recordings from the Pacific Northwest region by more than 10-fold. Thus, empirical attenuation relationships (Crouse, 1991; Atkinson, 1997;

Youngs *et al.*, 1997), which have been traditionally used to estimate both deterministic and probabilistic ground-motion hazard in the Pacific Northwest for interface events have, by necessity, been derived from strong-motion recordings from other subduction zones (e.g., Japan, Chile, and Mexico). Furthermore, the largest earthquake in these data is only a  $M$  8.2 earthquake (Crouse, 1991). Whether these relationships are appropriate for the Pacific Northwest in terms of rupture plane geometry, earthquake stress drops, crustal attenuation ( $Q$ ), velocity structure, and other source and path parameters is uncertain. The validity of extrapolating these relationships up to  $M$  9, the magnitude of the most recent earthquake in 1700 (Satake *et al.*, 1996), is also a significant issue, especially for engineering design purposes.

### Existing Attenuation Relationships

For the probabilistic National Seismic Hazard Maps (Frankel *et al.*, 1996), the Youngs *et al.* (1997) empirical attenuation relationship was the only subduction zone relationship used for the modeling of ground motion from the Cascadia subduction zone megathrust source. Youngs *et al.* (1997) stated, however, that their relationships are poorly constrained at small distances (<50 km) because of a lack of data from more than a few earthquakes. To aid in estimating ground motions at these short distances from large subduction events, Youngs *et al.* (1997) utilized the same stochastic finite-fault model that was used in this study to simulate ground motions for **M** 7.0, 8.0, and 8.5 megathrust earthquakes. Their simulations predicted higher near-field ground motions than those extrapolated from empirical data. The simulations predicted ground motions that were comparable in amplitude to the ground motions predicted by empirical attenuation relationships for shallow-crustal reverse-faulting earthquakes (e.g., Sadigh *et al.*, 1993). Thus, for short distances, Youngs *et al.* (1997) suggested that higher ground motions be considered than those empirically predicted. Based on this recommendation, the 1996 National Hazard Maps also included the Sadigh *et al.* (1993) empirical attenuation relationship for reverse faulting for modeling ground motions from Cascadia subduction zone interface events.

Estimating ground motions at short distances (<50 km) for a Cascadia megathrust rupture is important in the Pacific Northwest. Based on a model of megathrust rupture extending halfway into the transition zone of Flück *et al.* (1997), horizontal distances from the eastern edge of a Cascadia megathrust rupture to the coast range from zero at Cape Mendocino, California; Cape Blanco, Oregon; and along the western Washington coast to about 40–50 km along the northern Oregon coast (Wong and Silva, 1998). The heavily urbanized areas of Puget Sound region in Washington and the Portland metropolitan region and the Willamette Valley in Oregon are at approximate horizontal distances of 100–160 km from the Cascadia megathrust.

The attenuation relationships of Crouse (1991), which are appropriate for firm soil conditions, do not differentiate between the ground motions from interface and intraplate earthquakes. This is a significant consideration because it appears that ground motions from these two types of subduction zone earthquakes differ in amplitude for a given magnitude and distance (Youngs *et al.*, 1988, 1997).

Atkinson (1997) and Atkinson and Boore (1997) developed attenuation relationships for the Cascadia region, but they did not distinguish among crustal, intraplate, and megathrust events. The Atkinson (1997) relationships are empirically derived, whereas those of Atkinson and Boore (1997) are based on a stochastic point-source numerical ground-motion model.

Because none of the aforementioned empirical attenu-

ation relationships are based on Cascadia megathrust strong-motion records and because they are extrapolated above **M** 8.2, we have developed a set of attenuation relationships appropriate for megathrust earthquakes from **M** 8.0 to 9.0 in the Cascadia subduction zone. In seismic-hazard analysis, it is often desired to use multiple attenuation relationships to incorporate the epistemic uncertainty in estimating ground motions. Our relationships provide an alternative approach to empirically based ground-motion estimation. For example, in the development of probabilistic microzonation ground shaking maps for the Portland, Oregon, metropolitan area, ground motions from the Cascadia megathrust were estimated using the Youngs *et al.* (1997) relationships and the stochastic finite-fault model-based relationship described in this article (Wong *et al.*, 2000).

The attenuation relationships developed in this study are for 5%-damped, horizontal response spectral acceleration. Because these relationships were originally developed for use in preparing the Portland microzonation hazard maps, the input parameters described subsequently are most appropriate for northwestern Oregon and southwestern Washington. However, we believe they are also applicable to many other areas along the Cascadia subduction zone.

### Approach

The computed ground motions used in the attenuation relationships are based on a stochastic finite-fault ground-motion model developed by Silva *et al.* (1990). The target earthquake ground motions are modeled as a combination of smaller subevent earthquakes occurring over the target rupture plane. This is the same model used by Youngs *et al.* (1997) in their development of the empirical attenuation relationship for subduction-zone earthquakes. A revised version of this model is described in detail by Schneider *et al.* (1993) and Silva *et al.* (1998).

This stochastic finite-fault ground-motion model has been used to simulate site-specific ground motions for engineering design for **M** 8.5–9.0 Cascadia megathrust events in the Pacific Northwest (Silva *et al.*, 1998; Wong and Silva, 1998). The advantage of employing finite-fault numerical simulations is that unlike empirical attenuation relationships, which contain an uneven sampling of site and source geometries based on the available strong-motion dataset, finite-fault effects such as rupture propagation, directivity, and source-to-site geometry can be systematically accounted for.

For this study the stochastic finite-fault model was used to simulate subduction zone megathrust events of **M** 8.0, 8.5, and 9.0 on the Cascadia subduction zone. Uncertainties in source, path, and site parameters are included in the computations through parametric variations. Uncertainties in the regression of the simulated data are added to the modeling uncertainty to produce 16th, 50th (median), and 84th percentile attenuation relationships.

### Model Validation

The stochastic finite-fault model has been validated for crustal earthquakes using 15 earthquakes recorded at about 500 sites (W. J. Silva *et al.*, unpublished report, 1997). For subduction zone earthquakes, the stochastic finite-fault model has been validated using the recorded ground motions from two large subduction zone megathrust earthquakes (Humphrey *et al.*, 1993). The first large subduction earthquake used in the validation of the finite-fault modeling was the 19 September 1985 M 8.0 Michoacan, Mexico, earthquake. The slip model of Mendez and Anderson (1991) was used to model the 5%-damped response spectral accelerations at 14 rock sites. Epicentral distances to the sites ranged from 20 to 400 km, and shortest distances to the rupture surface range from 15 to 250 km. Site-specific kappa values (Humphrey and Anderson, 1993; Silva and Darragh, 1995) were used in the modeling process for each site. A local crustal velocity model (Somerville *et al.*, 1991) and a local crustal damping model of Humphrey and Anderson (1993) were used for the modeling of the Michoacan data. In general the stochastic finite-fault ground motions agree favorably with the recorded ground motions at periods of 0.02 to 10–20 sec. For the four closest sites, the model predicts higher ground motions than were recorded. This type of overprediction of ground motion from megathrust events at short distances has been previously noted by Youngs *et al.* (1997). A quantitative measure of the goodness-of-fit will be discussed subsequently for the combined Michoacan and Valpariso earthquakes.

Compared to the Michoacan earthquake, the 3 March 1985 M 8.0 Valpariso, Chile, earthquake has substantially fewer recorded ground motions and less information on the recording stations for the validation of the model. There were six rock strong ground motion stations ranging in rupture distance from 39 to 120 km that were modeled from this earthquake. The slip model of Somerville *et al.* (1991) was used in the modeling. The Michoacan regional crustal damping model (Humphrey and Anderson, 1993) and the crustal amplification factors of Boore (1986) were used for the Valpariso earthquake because of a lack of an appropriate crustal-damping model for the region. Site-specific kappa values were estimated based on the comparison of response spectral shapes with the spectral shapes for known kappa values (Silva and Darragh, 1995). The agreement between the recorded ground motions and the model ground motions are similar to the agreement for the Michoacan data.

To provide a quantitative measure of the uncertainties in the ground-motion predictions, a simple goodness-of-fit was performed at each spectral period. The modeling uncertainty is the average at each frequency of the difference of the natural logarithms of the observed ground motions and the model-predicted ground motions. The uncertainty for the combined Michoacan and Valpariso data is shown in the top part of Figure 1. For frequencies greater than about

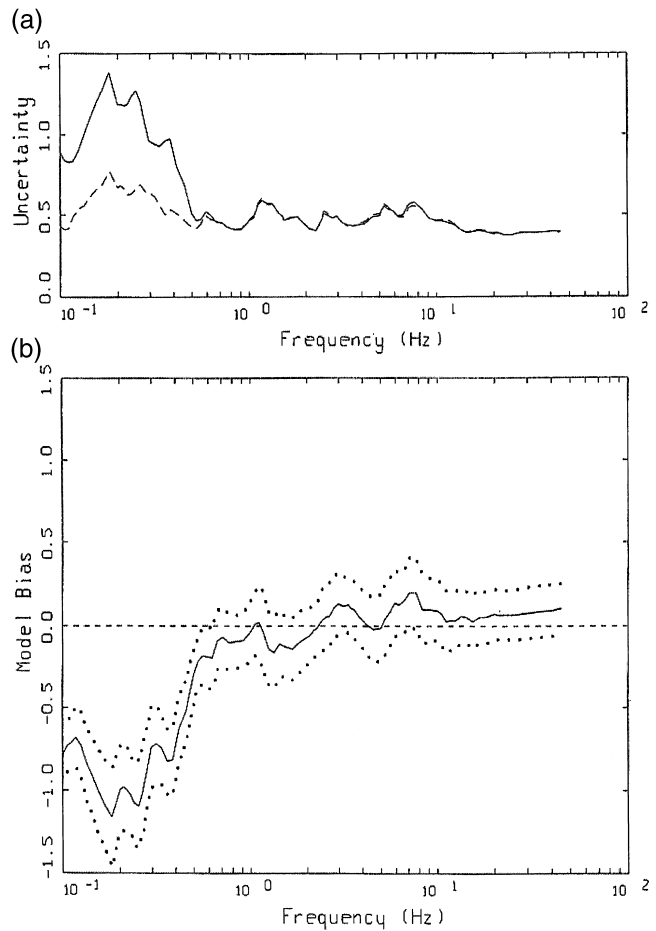


Figure 1. (a) Modeling uncertainty (solid) and bias-corrected modeling uncertainty (dashed) (both  $\sigma_{ln}$ ) and (b) model bias with 90% confidence limits (dotted line) computed for the combined data from the 1985 Michoacan, Mexico, and Valpariso, Chile, earthquakes.

1 Hz, the total modeling uncertainty ( $\sigma_{ln}$ ) is low, generally below about 0.4. The modeling bias (Abrahamson *et al.*, 1990) is shown in the lower plot in Figure 1 for the combined data along with 90% confidence intervals (dotted lines). Above 0.6 Hz, the bias is essentially zero. The negative bias values for longer periods (i.e., frequencies less than about 0.5 Hz) indicate an overprediction of the ground motions by the model compared to the recorded ground motions. The bias-corrected modeling uncertainty (Abrahamson *et al.*, 1990) is shown in the top part of Figure 1 as the dashed line. This uncertainty will be included with the parametric regression uncertainty to give a total uncertainty in the attenuation relationship.

### Input Parameters

The seismic source, path, and site parameters used in the stochastic finite-fault ground-motion simulations are described in the following sections.

**Seismic Source.** The rupture planes for the M 8.0, 8.5, and 9.0 events were modeled as being 90 km wide and 150, 450, and 1100 km long, respectively (Fig. 2). The width of the potential megathrust rupture varies along the length of the subduction zone from approximately 50 km in southern Oregon and the northwest corner of California to about 150 km in the Olympic Peninsula (Hyndman and Wang, 1995; Flück *et al.*, 1997). The 90-km width is an average value assuming that rupture involves the locked zone and extends halfway into the transition zone of the Flück *et al.* (1997) model of the Cascadia subduction zone (Wong and Silva, 1998). This width is the same width used in the National Seismic Hazard Map modeling for the Cascadia subduction zone (Frankel *et al.*, 1996). The extent to which the transition zone is involved in coseismic rupture is highly uncertain, and the validity of the Cascadia subduction zone model of Flück *et al.* (1995) and its predecessors (e.g., Hyndman *et al.*, 1997) is still being evaluated (Wong and Silva, 2000).

The rupture planes were modeled as rectangular areas (Fig. 2). To define the lengths of the ruptures, the Wells and Coppersmith (1994) empirical relationship between rupture area and magnitude was used. Using an empirical relationship for rupture area and magnitude derived from subduction zone earthquakes (Abe, 1981, 1984) yields very similar earthquake fault areas to that of Wells and Coppersmith (1994). The rupture planes were modeled as dipping 9° to

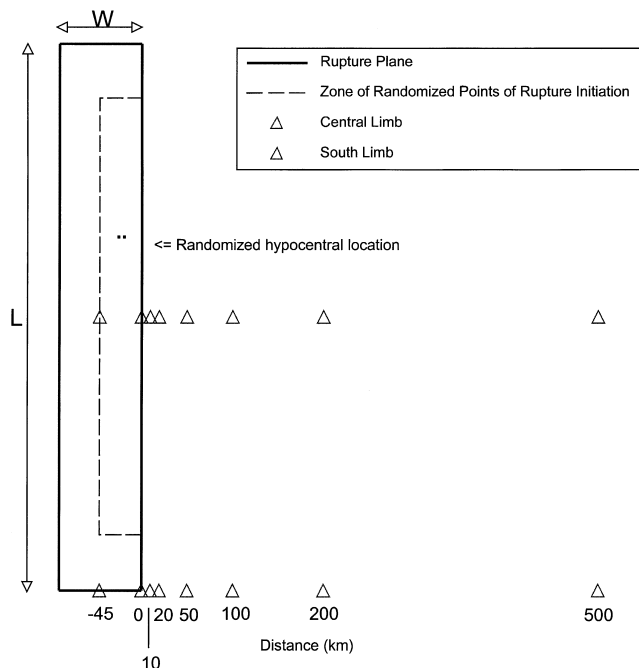


Figure 2. Megathrust rupture and site geometry used to calculate finite-fault stochastic ground motions used in regressing attenuation relationships. The rupture initiation location is constrained to be within the dashed box. Ground motions are computed for the 16 sites shown as triangles along the two limbs of stations.

the east, which is an average value for the central portion of the subduction zone. The top of the rupture plane was placed at a depth of 5 km, and the bottom was placed at about 20 km based on the model of Wong and Silva (1998) for northwestern Oregon and southwestern Washington.

For each simulation, a different randomized slip model was used. These models were generated using a scheme that preserves the number and size of asperities given a rupture area to observed slip models from past earthquakes. The amplitude of slip was also varied over the fault plane. This slip generation scheme is based on a suite of actual slip distributions determined from inversions (Abrahamson *et al.*, 1994). Reverse slip was assumed with a variation in the rake angle of 30°.

In addition to randomized slip models, the point of rupture initiation was also randomized, although it was constrained to be located in an area occupying the lower half of the rupture and within 10% from the ends (dashed box in Fig. 2). The average of the suite of random hypocenters was selected to be approximately in the center of the north-south extent of the fault plane and three-fourths the width down the fault plane.

**Crustal Model and Attenuation.** A frequency-dependent  $Q(f)$  relationship for the Cascadia subduction zone region was used in the simulations where  $Q(f) = Q_0 f^\eta$ . Values of  $Q_0$  of 380 and  $\eta$  of 0.39 were adopted from Atkinson's (1995) estimate for western Washington and southwestern Canada. The parameter  $Q_0$  was randomly varied assuming a  $\sigma_{ln}$  of 0.40. The parameter  $\eta$  was held fixed at 0.39 in the ground-motion simulations.

A *P*-wave crustal model was developed in this study based on the models of Trehu *et al.* (1994), Cohee *et al.* (1991), and Ludwin *et al.* (1991). Based on this model, *S*-wave velocities were calculated assuming a Poisson's ratio of 0.25. These models are listed in Table 1, along with the densities from Couch and Riddihough (1989).

**Site Model.** Ground motions for both rock-and soil-site

Table 1  
Crustal Model for Northwest Oregon–Southwest Washington

Depth* (km)	$V_p$ (km/sec)	$V_s$ (km/sec)	$\rho^\dagger$ (g/cm <sup>3</sup> )
0.0	0.29–3.03	0.17–1.75	2.00–2.20
0.3	3.46	2.00	2.30
1.5	4.50	2.60	2.50
3.5	5.10	2.94	2.60
5.5	5.70	3.29	2.65
8.0	6.30	3.64	2.70
11.5	6.60	3.80	2.80
16.0	6.73	3.89	2.85
20.0	6.86	3.96	2.90
25.0	6.95	4.01	2.90
41.0	7.80	4.50	3.00

\*Depth to top of layer.

†Densities from Couch and Riddihough (1989).

conditions were generated. We assumed that the top 0.3 km of the crustal velocity model (Table 1) for rock-site conditions corresponded to Columbia River basalt (CRB), which occurs throughout a large portion of southwestern and south-central Washington and northwestern Oregon. The CRB was modeled with an *S*-wave velocity gradient based on Mabey and Madin (1993). The 300-m-thick soil profile was developed based on an analysis of geologic borehole profiles in the Portland region for Quaternary alluvium surface soil conditions. The average shear-wave velocities for the rock and soil profiles in the upper 30 m are 363 m/sec and 182 m/sec, respectively. These profiles were randomized for the ground-motion simulations using a correlation model for seismic velocities and layer thicknesses developed by G. Toro (W. J. Silva *et al.*, unpublished report, 1997). A total low-strain kappa value of 0.04 sec was used for both the rock and soil sites. This base kappa value was also randomized assuming a  $\sigma_{ln}$  of 0.30 (Electric Power Research Institute [EPRI], 1993) for the ground-motion simulations.

The top 150 m of both the rock and soil profiles were modeled with nonlinear rock and soil site properties (EPRI, 1993). The relatively low *S*-wave velocities (170 m/sec) near the surface for the CRB suggest that this profile will produce ground motions that are similar to shallow soil site conditions, typical of weathered CRB. As a result, high-frequency motions, such as peak acceleration, may be expected to be higher on CRB than stiffer rock-site conditions, all else being equal (EPRI, 1993; W. J. Silva *et al.*, unpublished report, 1999).

## Results

Simulations for **M** 8.0, 8.5, and 9.0 events were performed at eight sites along each of two east–west profiles (Fig. 2). One profile was placed at the southern end of the rupture plane, and the other was placed at the center of the rupture plane. Sites along each limb were placed directly along the centerline of the rupture plane (at approximately 45-km distance) and above its eastern edge. The remaining six sites for each limb were placed at horizontal distances of 10, 20, 50, 100, 200, and 500 km (Fig. 2).

A total of 20 simulations were made for each magnitude, distance, and site location, and the resulting 5%-damped acceleration response spectra were fitted with an attenuation functional form that accommodates magnitude-dependent ground-motion saturation and far-field distance-dependent fall-off. A weighting scheme was applied to the data from each limb of stations to control the magnitude saturation at short distances, thereby preventing the regression model from predicting lower ground motions for larger magnitude events at the same short distances. If this weighting scheme constraint was not used in the regression procedure, the results based on the simulations of the **M** 8.5 and 9.0 events would produce lower ground-motion estimates at short distances (i.e., for sites located over the fault plane) than those from the **M** 8.0 event.

This oversaturation of ground motion is observed in the preferred nonparametric empirical attenuation model of Anderson (1997) for subduction events recorded in the Guerrero array in Mexico. The third model presented by Anderson (1997), which is not significantly different statistically than the preferred model and contains greater smoothing of the data, has magnitude saturation but not oversaturation. Other published attenuation models for both subduction (e.g., Youngs *et al.*, 1997) and crustal (e.g., Abrahamson and Silva, 1997) earthquakes do not have an oversturation of ground motion. From an engineering design viewpoint, any attenuation model that produces lower ground motions for larger events at the same distances is difficult to justify, given our current understanding of earthquake ground motions. Although limited in the empirical data from large earthquakes at short distances, the Youngs *et al.* (1997) attenuation relationship, as well as other crustal attenuation relationships (e.g., Abrahamson and Silva, 1997), were developed with the constraint of ground-motion saturation but not oversaturation.

For the **M** 9.0 event, the fault length is 1100 km, which means that the two limbs of stations used in the simulations are separated by 550 km. For the limb of stations located at the southern end of the rupture plane, the ground motions tend to be lower in amplitude and longer in duration than for the stations located along the middle limb because of the large separation distance from the southern end of the fault plane to the rest of the rupture plane. This type of variation in ground motions is also observed in large crustal earthquakes (e.g., 1992 Landers, California) due to the propagating rupture along the finite-rupture plane. Hence, for the shorter rupture plane of the **M** 8.0 (150 km long) event, these effects are not as pronounced. The effect is also reduced as the stations are located further to the east of the rupture plane and the rupture distance increases. Based on these factors and the constraint of the model for saturation and not oversaturation, the modeled ground motions from the two limbs of the **M** 8.0 event were weighted equally. For the **M** 8.5 event, weights of 0.7 and 0.3 were assigned to the central and southern limb of stations, respectively, and 0.86 and 0.14 to the **M** 9.0 event.

The simulation results were fit to a functional form of

$$\ln Y = C_1 + C_2 * M + (C_3 + C_4 * M) * \ln[R + \exp(C_5)] + C_6 * (M - 10)^3, \quad (1)$$

where *Y* is the peak ground-motion parameter, *R* is closest distance to the rupture plane, and  $C_1$ – $C_6$  are coefficients fit to the data for rock (Table 2) and soil site conditions (Table 3). The total uncertainty in the regression results are also listed in Tables 2 and 3, where these values include the vector sum of the modeling and parametric uncertainty. The regressions were performed out to a period of 5.0 sec.

Figure 3 illustrates the range of simulated peak horizontal ground accelerations (PGA) for rock-site conditions

Table 2  
Coefficients and Standard Errors for Rock-Site Conditions

Period (sec)	C <sub>1</sub>	C <sub>2</sub>	C <sub>3</sub>	C <sub>4</sub>	C <sub>5</sub>	C <sub>6</sub>	Param. Sigma	Model Sigma	Total Sigma
PGA	21.0686	-1.7712	-5.0631	0.4153	4.2	0.0017	0.6083	0.3926	0.7240
0.010	20.9932	-1.7658	-5.0404	0.4132	4.2	0.0226	0.6031	0.3926	0.7195
0.020	21.072	-1.772	-5.0529	0.4142	4.2	0.0025	0.6036	0.3926	0.7195
0.025	21.152	-1.779	-5.0663	0.4154	4.2	0.0023	0.6042	0.3983	0.7235
0.032	21.366	-1.797	-5.1036	0.4187	4.2	0.0017	0.6062	0.3926	0.7221
0.040	17.525	-1.339	-4.8602	0.3868	4.2	-0.0318	0.5836	0.3818	0.6969
0.050	19.347	-1.519	-4.9731	0.3960	4.2	-0.0155	0.5908	0.3925	0.7086
0.056	20.774	-1.625	-5.1875	0.4118	4.3	-0.0155	0.5974	0.4052	0.7215
0.063	21.331	-1.672	-5.2561	0.4173	4.3	-0.0146	0.6028	0.4132	0.7302
0.071	24.221	-1.924	-5.6250	0.4478	4.4	-0.0071	0.6116	0.4042	0.7326
0.083	24.950	-1.979	-5.6696	0.4493	4.4	-0.0018	0.6337	0.4584	0.7815
0.100	30.005	-2.349	-6.3862	0.5009	4.7	-0.0019	0.6448	0.4668	0.7954
0.125	39.719	-3.090	-7.8541	0.6161	5.1	-0.0064	0.6654	0.5461	0.8605
0.143	43.414	-3.385	-8.3122	0.6513	5.2	-0.0001	0.6769	0.5225	0.8544
0.167	39.579	-2.957	-7.9723	0.6139	5.2	-0.0264	0.6810	0.5050	0.8478
0.200	39.345	-3.087	-7.6002	0.5972	5.1	0.0060	0.7034	0.5089	0.8679
0.250	37.690	-2.960	-7.3790	0.5842	5.1	-0.0023	0.7121	0.4539	0.8444
0.333	34.787	-2.899	-6.7855	0.5616	4.9	0.0256	0.7372	0.4764	0.8776
0.400	33.393	-2.776	-6.9595	0.5863	4.9	-0.0039	0.7110	0.5187	0.8801
0.500	29.159	-2.424	-6.2114	0.5216	4.7	0.0161	0.6745	0.4382	0.8039
0.769	15.279	-1.220	-4.3240	0.3618	3.9	-0.0011	0.6111	0.5611	0.8295
1.000	6.528	-0.406	-3.1991	0.2589	3.2	-0.0225	0.5898	0.4751	0.7567
1.667	7.467	-0.676	-2.6465	0.2193	2.8	0.0416	0.4931	0.4889	0.6943
2.000	8.657	-0.851	-2.7398	0.2339	2.8	0.0370	0.4666	0.4247	0.6305
2.500	6.637	-0.651	-2.3124	0.1879	2.8	0.0364	0.4163	0.5198	0.6657
5.000	8.013	-0.943	-2.4087	0.2154	2.3	0.0647	0.3931	0.6656	0.7730

Table 3  
Coefficients and Standard Errors for Soil-Site Conditions

Period (sec)	C <sub>1</sub>	C <sub>2</sub>	C <sub>3</sub>	C <sub>4</sub>	C <sub>5</sub>	C <sub>6</sub>	Param. Sigma	Model Sigma	Total Sigma
PGA	23.8613	-2.2742	-4.8803	0.4399	4.7	0.0366	0.3760	0.3926	0.5436
0.010	25.4516	-2.4206	-5.1071	0.4605	4.8	0.0372	0.3742	0.3926	0.5422
0.020	25.4339	-2.4185	-5.1044	0.4602	4.8	0.0370	0.3742	0.3926	0.5422
0.025	25.4200	-2.4168	-5.1026	0.4600	4.8	0.0369	0.3743	0.3983	0.5464
0.032	25.3849	-2.4127	-5.0977	0.4594	4.8	0.0366	0.3743	0.3926	0.5422
0.040	22.7042	-2.1004	-4.9006	0.4353	4.8	0.0164	0.3590	0.3818	0.5241
0.050	23.2948	-2.1619	-4.8855	0.4332	4.8	0.0263	0.3592	0.3925	0.5319
0.056	23.2165	-2.1528	-4.8744	0.4319	4.8	0.0255	0.3598	0.4052	0.5413
0.0625	24.7067	-2.2814	-5.0947	0.4509	4.9	0.0245	0.3607	0.4132	0.5480
0.070	24.9425	-2.3045	-5.0672	0.4476	4.9	0.0295	0.3609	0.4042	0.5413
0.083	26.5395	-2.4402	-5.3025	0.4677	5.0	0.0276	0.3617	0.4584	0.5835
0.100	29.9693	-2.7254	-5.8054	0.5098	5.2	0.0226	0.3654	0.4668	0.5926
0.125	35.6660	-3.1853	-6.6251	0.5769	5.5	0.0123	0.3821	0.5461	0.6665
0.143	50.7368	-4.5292	-8.7213	0.7649	5.9	0.0108	0.3923	0.5225	0.6532
0.167	55.6402	-4.9662	-9.5555	0.8435	6.0	-0.0070	0.3927	0.5050	0.6393
0.200	75.8218	-6.8396	-12.0687	1.0753	6.3	0.0096	0.4231	0.5089	0.6618
0.250	100.3357	-9.0324	-15.3511	1.3731	6.6	-0.0043	0.4472	0.4539	0.6371
0.330	71.7967	-6.4990	-11.6056	1.0415	6.2	0.0102	0.4324	0.4764	0.6431
0.400	67.3720	-6.1755	-11.1567	1.0167	6.1	0.0035	0.4243	0.5187	0.6699
0.500	56.0088	-5.1176	-9.5083	0.8632	5.9	0.0164	0.4305	0.4382	0.6139
0.770	26.3013	-2.4482	-5.3818	0.4957	4.8	0.0259	0.4601	0.5611	0.7256
1.000	17.2330	-1.5506	-4.3287	0.3930	4.2	0.0133	0.4599	0.4751	0.6606
1.670	11.9971	-1.1180	-2.9451	0.2639	3.7	0.0538	0.4781	0.4889	0.6837
2.000	17.9124	-1.7505	-3.8150	0.3574	4.1	0.0583	0.4628	0.4247	0.6276
2.500	16.1666	-1.5091	-3.7101	0.3344	4.1	0.0473	0.4193	0.5198	0.6676
5.000	7.4856	-0.8360	-2.0627	0.1779	-0.2	0.0821	0.4802	0.6656	0.8207

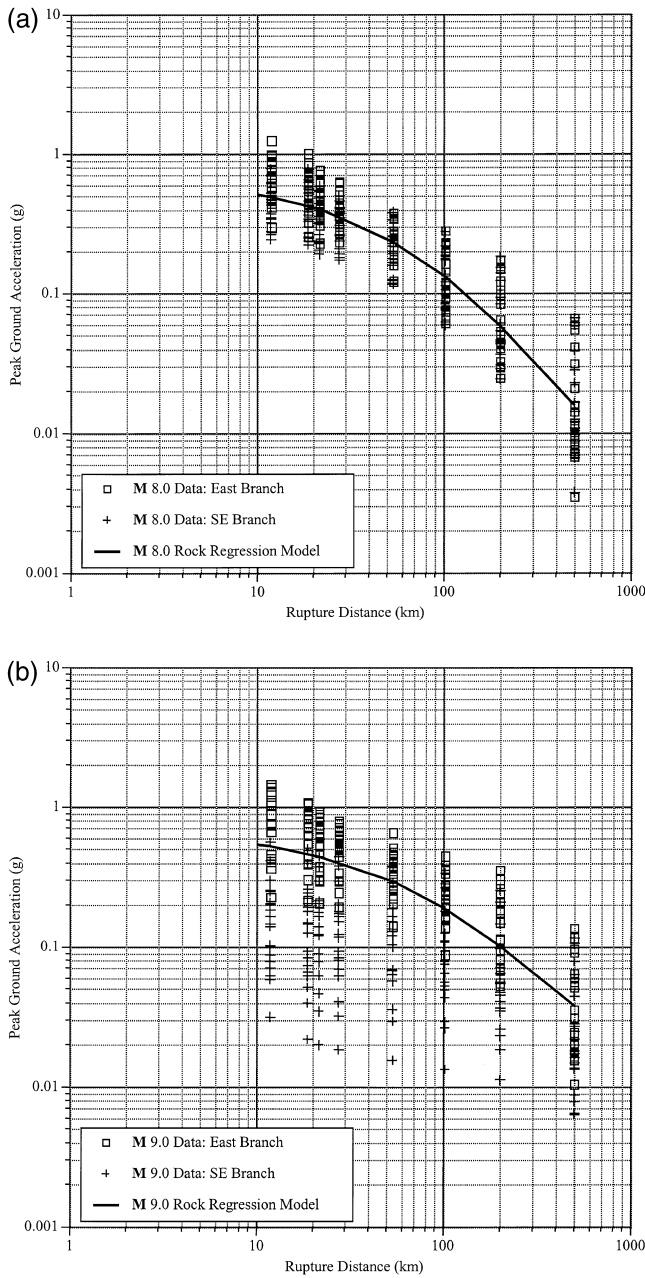


Figure 3. Regression of finite-fault simulations for (a) **M** 8.0 and (b) 9.0 earthquakes for rock-site conditions. Triangles represent results for the central limb and pluses for the southern limb indicating the lower simulated ground motions for the southern limb of stations.

for each site location profile and the best-fitting relationship for **M** 8.0 and 9.0 events. The **M** 9.0 simulations show a greater variability in PGA than do the **M** 8.0 events based on the larger separation distance of the two station limbs relative to the total length of the rupture plane, as discussed previously. The soil ground-motion simulations show the same variation in ground motion with magnitude and site locations.

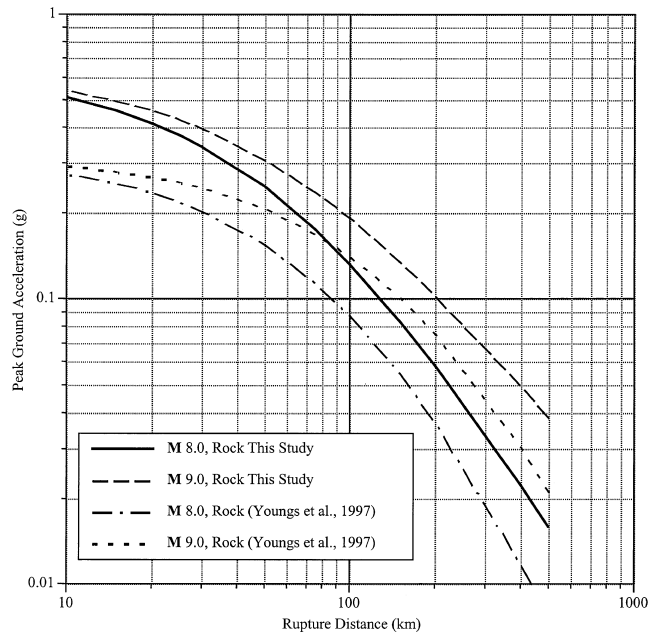


Figure 4. Comparison between Youngs *et al.* (1997) model and this model for peak horizontal acceleration for rock-site conditions for **M** 8.0 and 9.0.

The median PGA attenuation relationships for **M** 8.0 and 9.0 are shown on Figure 4. Due to the magnitude saturation constraint, the attenuation model predicts about 0.5g for both magnitudes at a distance of 10 km for rock-site conditions. This level of magnitude saturation is similar to the magnitude saturation observed in the Youngs *et al.* (1997) empirical attenuation curves, which are also plotted in Figure 4 for **M** 8.0 and 9.0. The median Youngs *et al.* (1997) curves are shown with a hypocentral depth of 16 km, which represents an average depth of rupture initiation used in the generation of the model ground motions. As noted by Youngs *et al.* (1997), the simulations exceed the empirical predictions by a factor of approximately 2 at distances less than 50 km. An approach using the equally weighted Youngs *et al.* (1997) and Sadigh *et al.* (1997) relationships, as recommended by R. Youngs (Geomatrix Consultants, personal comm., 1999), would result in PGAs of about 0.5g at 10 km, which is approximately equal to the value predicted by our relationship (Fig. 4). The simulations exceed the Youngs *et al.* (1997) predictions at longer distances.

Figure 5 is a plot of the PGA attenuation with rupture distance for soil-site conditions. Also shown are the Youngs *et al.* (1997) relationships for **M** 8.0 and 9.0 events. Both relationships predict similar PGA values at distance out to 100–150 km. At greater distances, the current relationship has a slower rate of ground-motion attenuation and consequently predicts larger PGA values. This difference in far-field attenuation can be attributable to the softer soil profile used in our ground-motion simulations when compared to the average soil profiles of the empirical data recorded at

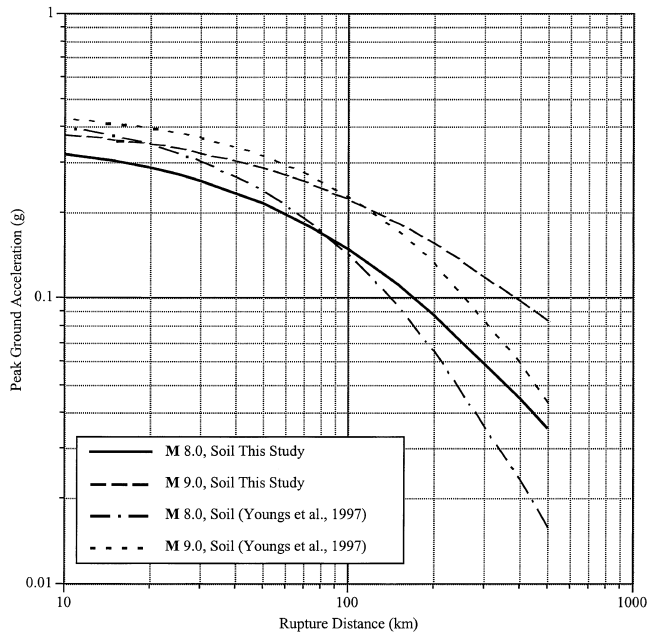


Figure 5. Comparison between Youngs *et al.* (1997) model and this model for peak horizontal acceleration for soil-site conditions for M 8.0 and 9.0.

large distances used in the Youngs *et al.* (1997) attenuation relationship.

Comparisons between the PGA attenuation relationships for both rock and soil from this study and the relationships from the previous finite-fault studies for the Cascadia megathrust (Youngs *et al.*, 1997) indicates a lower rate of attenuation and higher PGA values at longer distances (Fig. 4, 5). Youngs *et al.* (1997) used the Cohee *et al.* (1991) crustal velocity and the Humphrey and Anderson (1993) crustal attenuation model. These differ slightly from the models used in the current ground-motion simulations. Also, in the previous modeling, crustal amplification factors were applied based on the Cohee *et al.* (1991) velocity model, which has faster velocities than the model used in this study (Table 1). This faster velocity structure leads to smaller ground-motion amplification than the slower velocity structure model used in the present study. Analysis of subduction zone earthquake strong-motion data recorded on shallow stiff soil sites indicated approximately 50% higher peak accelerations than data recorded on rock sites (Geomatrix Consultants, unpublished report, 1993).

Median (5%-damped) response spectra for both rock and soil are shown in Figure 6 for a M 8.5 event at rupture distances of 50 and 100 km. The response spectra contain small peaks and valleys because the regression coefficients have not been smoothed. A comparison between the current rock spectra and the predicted rock spectra from the Youngs *et al.* (1997) attenuation model indicate a similar spectral shape, with our model predicting higher ground-motion val-

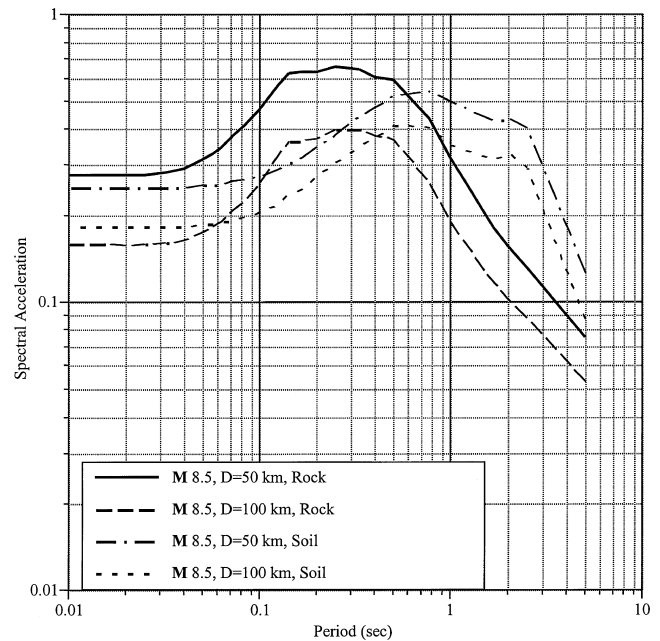


Figure 6. Horizontal median response spectra (5%-damped) for rock-and soil-site conditions for a M 8.5 earthquake at distances of 50 and 100 km estimated by the current model.

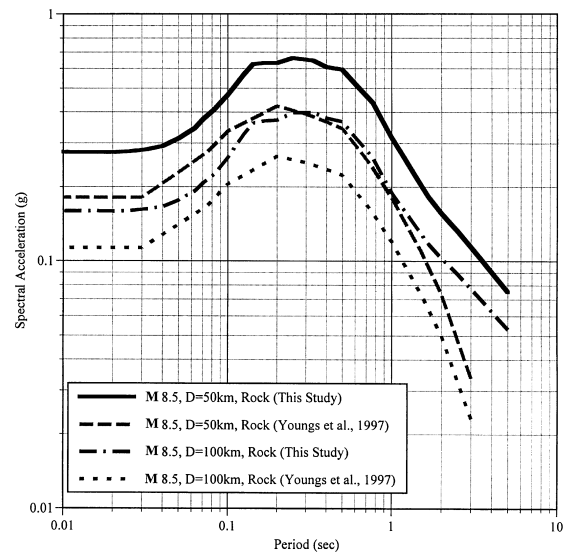


Figure 7. Comparison of horizontal median response spectra (5%-damped) between Youngs *et al.* (1997) model and this model for rock-site conditions for a M 8.5 earthquake at distances of 50 and 100 km.

ues (Fig. 7). Our model for soil-site conditions has a spectral peak at a longer spectral period (i.e., 0.7 sec) than either the Youngs *et al.* (1997) or Crouse (1991) attenuation models. This is an expected result based on the relatively soft soil profile used in the ground-motion simulations.

## Acknowledgments

This article was greatly improved based on the comments and suggestions by two anonymous reviewers. This study was supported by the U.S. Geological Survey under NEHRP Award 1434-HQ-96GR-02727. Our thanks to Rachel Griener, Fumiko Goss, and Melinda Lee for assisting in the preparation of this article.

## References

- Abe, K. (1981). Magnitude of large shallow earthquakes from 1904–1980, *Phys. Earth Planet. Interiors* **27**, 72–92.
- Abe, K. (1984). Complements to “Magnitudes of large shallow earthquakes from 1904–1980,” *Phys. Earth Planet. Interiors* **34**, 17–23.
- Abrahamson, N. A., W. J. Silva, and J. Schneider (1994). Variability of strong ground motion due to the variability of seismic slip distribution (abstract), *Seism. Res. Lett.* **65**, 35.
- Abrahamson, N. A., P. G. Somerville, and C. A. Cornell (1990). Uncertainty in numerical strong motion proceedings, in Proc. Fourth U.S. National Conference on Earthquake Engineering, Vol. 1, p. 407–416.
- Anderson, J. G. (1997). Nonparametric description of peak acceleration above a subduction thrust, *Seism. Res. Lett.* **68**, 86–93.
- Atkinson, G. M. (1995). Attenuation and source parameters of earthquakes in the Cascadia region, *Bull. Seism. Soc. Am.* **85**, 1327–1342.
- Atkinson, G. M. (1997). Empirical ground motion relations for earthquakes in the Cascadia region, *Can. J. Civ. Eng.* **24**, 64–77.
- Atkinson, G. M., and D. M. Boore (1997). Stochastic point-source modeling of ground motions in the Cascadia region, *Seism. Res. Lett.* **68**, 74–85.
- Boore, D. M. (1986). Short-period P- and S- wave radiation from large earthquakes: implications for spectral scaling relations, *Bull. Seism. Soc. Am.* **76**, 43–64.
- Cohee, B. R., P. G. Somerville, and N. A. Abrahamson (1991). Simulated ground motions for hypothesized  $M_w = 8$  subduction earthquakes in Washington and Oregon, *Bull. Seism. Soc. Am.* **81**, 28–56.
- Couch, R. W., and R. P. Riddihough (1989). The crustal structure of the western continental margin of North America, in *Geophysical Framework of the Continental United States*, L. C. Pakiser and W. D. Mooney (Editors), Geological Society of America Memoir 172, 103–128.
- Crouse, C. B. (1991). Ground motion attenuation equations for earthquakes on the Cascadia subduction zone, *Earthquake Spectra* **7**, 201–236.
- Electric Power Research Institute (1993). Guidelines for determining design basis ground motions, Electric Power Research Institute, Rept. EPRI TR-102293, 1–5.
- Flück, P., R. D. Hyndman, and K. Wang (1997). 3-D dislocation model for great earthquakes of the Cascadia subduction zone, *J. Geophys. Res.* **102**, 20,539–20,550.
- Frankel, A., C. Mueller, T. Barnard, D. Perkins, E. V. Leyendecker, N. Dickman, S. Hanson, and M. Hopper (1996). National seismic-hazard maps; documentation June 1996, *U.S. Geol. Surv. Open-File Rept* 96-532, 110 pp.
- Humphrey, J. R., and J. G. Anderson (1993). Shear wave attenuation and site response in Guerrero, *Bull. Seism. Soc. Am.* **82**, 1622–1645.
- Humphrey, J. R., W. J. Silva, and R. R. Youngs (1993). Factors influencing site-specific ground motion estimates for the 1985 M 8.1 Michoacan earthquake (abstract), *Seism. Res. Lett.* **64**, 17.
- Hyndman, R. D., and K. Wang (1995). The rupture zone of Cascadia great earthquakes from current deformation data and thermal regime, *J. Geophys. Res.* **100**, 22,133–22,154.
- Ludwin, R. S., C. S. Weaver, and R. S. Crosson (1991). Seismicity of Washington and Oregon, in *Neotectonics of North America: Geological Society of America Decade of North American Geology*, D. B. Slemmons, E. R. Engdahl, M. Zoback, and D. Blackwell (Editors) Decade Map, Vol. 1, 77–98.
- Mabey, M. A., and I. P. Madin (1993). Ground motion amplification map, Portland quadrangle, Oregon, in *Earthquake Hazard Maps of the Portland Quadrangle, Multnomah and Washington Counties, Oregon, and Clark County, Washington*, Oregon Department of Geology and Mineral Industries Geological Map Series GMS-79.
- Mendez, A. J., and J. G. Anderson (1991). The temporal and spatial evolution of the 10 September 1985 Michoacan earthquake as inferred from near-source ground-motion records, *Bull. Seism. Soc. Am.* **81**, 844–861.
- Sadigh, K., C.-Y. Chang, N. A. Abrahamson, S. J. Chiou, and M. S. Power (1993). Specification of long-period ground motions: updated attenuation relationships for rock site conditions and adjustment factors for near-fault effects, in *Proceedings ATC-17-1 Seminar on Seismic Isolation, Passive Energy Dissipation, and Active Control*, 59–70.
- Sadigh, K., C.-Y. Chang, J. A. Egan, F. Makdisi, and R. R. Youngs (1997). Attenuation relationships for shallow crustal earthquakes based on California strong motion data, *Seism. Res. Lett.* **68**, 180–189.
- Satake, K., K. Shimazaki, Y. Tsuji, and K. Ueda (1996). Time and size of a giant earthquake in Cascadia inferred from Japanese tsunami records of January 1700, *Nature* **179**, 246–249.
- Schneider, J. F., W. J. Silva, and C. L. Stark (1993). Ground motion model for the 1989 M6.9 Loma Prieta earthquake including effects of source, path, and site, *Earthquake Spectra* **9**, 251–287.
- Silva, W. J., and R. B. Darragh (1995). Engineering characterization of strong ground motion recorded at rock sites, Electric Power Research Institute, Rept. EPRI TR-102262.
- Silva, W., R. Darragh, C. Stark, I. Wong, J. Stepp, J. Schneider, and S. Chiou (1990). A methodology to estimate design response spectra in the near-source region of large earthquakes using the Band-Limited-White-Noise ground motion model, in *Proc. Fourth U.S. National Conference on Earthquake Engineering*, Vol. 1, 487–494.
- Silva, W. J., I. G. Wong, and R. B. Darragh (1998). Engineering characteristics of earthquake strong ground motions in the Pacific Northwest, in *Assessing Earthquake Hazards and Reducing Risk in the Pacific Northwest*, A. M. Rogers, T. J. Walsh, W. J. Kockelman, and G. R. Priest (Editors), *U.S. Geol. Surv. Profess. Pap.* 1560, Vol. 2, 313–324.
- Somerville, P. G., M. Sen, and B. Cohee (1991). Simulation of strong ground motions recorded during the 1985 Michoacan, Mexico, and Valparaiso, Chile, earthquakes, *Bull. Seism. Soc. Am.* **81**, 1–27.
- Trehu, A. M., I. Asudeh, T. M. Brocher, J. H. Luetgert, W. D. Mooney, J. L. Nabelek, and Y. Nakamura (1994). Crustal architecture of the Cascadia forearc, *Science* **266**, 237–242.
- Wells, D. L., and K. J. Coppersmith (1994). New empirical relationships among magnitude, rupture length, rupture width, and surface displacement, *Bull. Seism. Soc. Am.* **84**, 974–1002.
- Wong, I. G., and W. J. Silva (1998). Earthquake ground shaking hazards in the Portland and Seattle metropolitan areas, in *Geotechnical Earthquake Engineering and Soil Dynamics III*, P. Dakoulas, M. Yegian, and R. D. Holtz (Editors), American Society of Civil Engineering Geotechnical Special Publication ASCE, no. 75, Vol. 1, 66–78.
- Wong, I. G., and W. J. Silva (2000). Predicting great earthquake ground shaking in the Pacific Northwest from the Cascadia subduction zone, in *Penrose Conference 2000: Great Cascadia Earthquake Tricentennial*, Program Summary and Abstracts, Oregon Department of Geology and Mineral Industries Special Paper 33, 141–143.
- Wong, I. G., W. J. Silva, J. Bott, D. Wright, P. Thomas, N. Gregor, S. Li, M. Mabey, A. Sojourner, and Y. Wang (2000). Earthquake scenario and probabilistic ground shaking maps for the Portland, Oregon metropolitan area, Oregon Department of Geology and Mineral Industries Interpretive Map Series IMS-16, scale 1:62,500, 11 sheets with 16 pp. text.
- Youngs, R. R., S. J. Chiou, W. J. Silva, and J. R. Humphrey (1997). Strong ground motion attenuation relationships for subduction zone earthquakes, *Seism. Res. Lett.* **68**, 58–73.

Youngs, R. R., S. M. Day, and J. P. Stevens (1988). Near-field motions on rock for large subduction zone earthquakes, in *Earthquake Engineering and Soil Dynamics II: Recent Advances in Ground Motion Evaluation*, American Society of Civil Engineering Geotechnical Special Publication No. 20, ASCE, 445–462.

Pacific Engineering and Analysis  
311 Pomona Avenue  
El Cerrito, CA 94530  
(N.J.G., W.J.S.)

URS Corporation  
500 12th Street, Suite 200  
Oakland, CA 94607  
(I.G.W.)

Geomatrix Consultants  
2101 Webster Street  
Oakland, CA 94612  
(R.R.Y.)

Manuscript received 25 February 2002.